Mean and fluctuating velocity fields of a diamond turbulent jet

2013 Chinese Phys. B 22 034701

(http://iopscience.iop.org/1674-1056/22/3/034701)

Mean and fluctuating velocity fields of a diamond turbulent jet*

Xu Min-Yi(徐敏义)[a)b)], Zhang Jian-Peng(张健鹏)[a)], Mi Jian-Chun(米建春)[a)†], Nathan G. J.[c)], and Kalt P. A. M.[c)]

[a)] *State Key Laboratory of Turbulence & Complex Systems, College of Engineering, Peking University, Beijing* 100871, *China*
[b)] *Marine Engineering College, Dalian Maritime University, Dalian* 116026, *China*
[c)] *Centre for Energy Technology and School of Mechanical Engineering, University of Adelaide, SA* 5005, *Australia*

(Received 26 June 2012; revised manuscript received 7 August 2012)

The present paper reports the first investigation on a turbulent jet issuing from a diamond orifice (hereafter termed a "diamond jet") with an aspect ratio of 1.7. Velocity measurements were conducted in the transitional region, and the exit Reynolds number of the jet was 50000. For comparison, a round jet with identical normalized boundary conditions was also measured. It is shown that the diamond jet decays and spreads faster than the round jet does over the measured flow region. The axis-switching phenomenon is observed in the diamond jet. Although both jets display primary coherent structures in the near field, these structures are found to break down more rapidly in the diamond jet, due to the higher three-dimensionality of the flow. Moreover, the streamwise components of the Reynolds normal stress and all the shear stresses reach their maxima around the location of the maximal mean shear while the maxima of the lateral components of the Reynolds normal stresses occur around the centreline of the jet.

Keywords: turbulent jet, non-circular jet, PIV measurement, jet entrainment

PACS: 47.27.wg, 47.80.Cb, 47.85.lk **DOI:** 10.1088/1674-1056/22/3/034701

1. Introduction

Noncircular jets (e.g., elliptical, rectangular, triangular jets) have been extensively studied over the past four decades due to their important roles in fundamental jet research and wide-range industrial applications. The typical reason is that these jets exhibit higher entrainment rates of ambient fluid than comparable round jets.[1–28]

The increase in entrainment of noncircular jets has been found to be strongly related to the curvature difference of the nozzle exit (constant curvature for circular exit and non-uniform curvatures for noncircular one), and the instability produced by the sharp corners.[29] According to Gutmark and Grinstein,[29] the above two factors will cause asymmetric distributions of the pressure and mean flow field, which accelerate the three-dimensionality of the flow structures, resulting in an enhancement in mixing eventually. The axis-switching phenomenon has been reported for elliptic and rectangular jets with aspect ratios above 1 and for triangular jets. The azimuthal curvature discrepancy of the initial vortical structures produces non-uniform self-induction and three-dimensionality. Thus, it causes the jets to spread in the plane more rapidly through the minor axis (i.e., short axis of symmetry) than through the major axis. As these kinds of jets proceed downstream, their mean-flow cross-sections tend to switch the minor and major axes at a certain distance from the nozzle exit (see, e.g., Refs. [16] and [29]). For corner-containing configurations, the corners can promote the formation of fine-scale streamwise vortices and thus enhance fine-scale turbulence.[1,6] The above phenomena have also been observed in many numerical simulations of noncircular jets.[9,10]

However, to the best of our knowledge, the flow field of a turbulent jet issuing from a diamond-shaped nozzle (hereafter termed a "diamond jet") has not yet been reported. Therefore, the present paper aims to report detailed measurements in the near and transition regions of a diamond jet, and make comparisons with a round jet. More specifically, we focus on the investigate the instantaneous and mean-flow fields, as well as the Reynolds stresses of the jets. The practical objective of this work is to provide new opportunities for optimizing the wide-range engineering applications that utilize jet flows.

2. Experimental details

Our experiments were carried out in the University of Adelaide using a similar setup to that of Mi *et al.*,[22,24] and hence only a brief description is provided here. Figure 1(a) shows the air supply tube of 25.4 mm in diameter and 1000 mm in length, to which an orifice plate (OP) was attached. Figures 1(b) and 1(c) present the shape and dimension of the two OPs, respectively. Both the nozzles have nearly identical equivalent diameter $D_e(\equiv 2(A\pi^{-1})^{1/2})$ of about 12 mm, with A being the area of the orifice. However, their hydraulic diameters $D_h(\equiv 2A/P_w$, with P_w being the wetted perimeter) are quite different, as indicated in the caption of Fig. 1 together with the aspect ratios (AR), i.e., the ratio of the long to short axis of symmetry.

*Project supported by the National Natural Science Foundation of China (Grant Nos. 11072005 and 10921202).
†Corresponding author. E-mail: jcmi@coe.pku.edu.cn

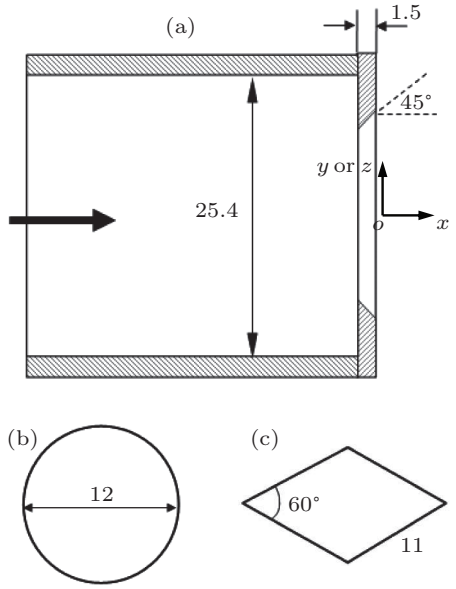

Fig. 1. (a) Air supply tube and attached orifice plate; (b) round exit: $D_e = D_h = 12$ mm and $AR = 1$; (b) diamond-shaped exit: $D_e = 11.6$ mm, $D_h = 9.57$ mm, $D_e/D_h = 1.21$, and AR = 1.7.

The flow rate of the tube was measured by using a pressure gauge with an accuracy of $\pm 5\%$ for calculating the jet's bulk-mean exit velocity and Reynolds number. The good axial symmetry of the tube flow from each OP was supported by the mean velocity at the tube exit which had different orientations.[22] Both jets were measured at the same Reynolds number of Re = 50000, where $\mathrm{Re} \equiv U_e D_e/\nu$, with U_e being the exit bulk velocity (≈ 90 m/s) and ν the kinematic viscosity of fluid.

The velocity measurements were accomplished by particle image velocimetry (PIV) with a Quantel Brilliant Twins double-head Nd:YAG laser at a frequency of 10 Hz, power of 250 mJ per pulse, and wavelength of 532 nm. More details of the measurement system can be found in Ref. [22]. The temporal separation of laser pulses was adjusted from 10 to 40 s, depending on the flow field. A MegaPlus ES1.0 camera with a 1008×1018 pixel array was operated in triggered double exposure mode to take 100 mm×100 mm images of the flow field. The collection optics comprised of a Nikon ED 70-300 mm (set to 110 mm) telephoto lens coupled to the camera C-mount with an adapter. The thickness of the laser light sheet was about 1 mm. The time delay between laser pulses was selected so that the interrogation region could be set to 32×32 pixels, with a 50% offset. This results in an effective resolution for the velocity measurements of 3 mm×3 mm. The nozzle was vertically placed so that our measurements covered the region $0 < x < 17D_e$, where x is the downstream distance from the orifice plate (see Fig. 1).

All statistical fields of velocity were obtained from an ensemble of 500 instantaneous vector fields. Statistical convergence was confirmed by down-sampling as reported by Mi *et al.*[22] The errors of the results obtained around the mean velocity half-width (see the definition in Section 3.1) at $x/D_e = 8$ are: $E_{[U]} \approx \pm 1.5\%$ (the error of the mean velocity); $E_{[<u^2>^{1/2}]} \approx \pm 2.5\%$, and $E_{[<v^2>^{1/2}]} \approx \pm 2.6\%$ (the errors of the root-mean-square (RMS) velocity fluctuations); $E_{[R_{1/2}]} \approx \pm 1.5\%$ (the error of the half-width of the mean velocity).

3. Results and discussion

3.1. Instantaneous velocity field

Figures 2(a) and 2(b) show the typical instantaneous velocity vectors (black arrows) and the magnitude contours (color) at $x/D_e \leq 8.2$ in the two symmetric planes of the diamond jet, i.e., the $x-y$ and $x-z$ planes. The comparable view through the central plane of the round jet is shown in Fig. 2(c). Clearly, each jet exhibits an oscillating manner that reflects the interaction between the jet and ambient fluid. In addition, the highest velocity, red but discontinuous in the contours, occurs in the central region of each jet, which results from the induction of the ambient fluid by the large-scale primary coherent structures. Considering that the average convection velocity of large-scale primary coherent structures in the near field of the round jet is approximately $0.6U_e$,[30] we calculated the streamlines of the instantaneous flow field under a translating coordinate with a speed of $0.6U_e$. Obviously, the instantaneous structures visualized by the streamlines match well with the vorticity contours of the flow field, indicating that the flow structures of jet can be easily and approximately visualized by this "streamline method". We have assessed the sensitivity of the resulting streamlines by using different values of assumed "convection" velocities from $0.4U_e$ to $0.7U_e$ and no significant difference was found.

Figures 3(a)–3(c) show that the primary vortical structure occurs from $x/D_e \approx 0.1$ in both the diamond and round jets. Generated by the roll-up of the initial shear layer, these vortical structures dominate the initial growth and entrainment of ambient fluid in jets.[9] It is clear that these structures are discernible in the range of $1 \leq x/D_e \leq 4$ in the diamond jet and $1 \leq x/D \leq 7$ in the round jet. This difference suggests that the underlying structure in the diamond jet is more three-dimensional than those in the round jet. It also suggests that the jet entrainment rate of the diamond jet may be higher than that of the round jet. In addition, figures 2 and 3 also appear to show the fundamental difference between underlying flow structures of the jets. Although both the diamond and round jets spread downstream and mix with ambient fluid, those processes appear to take place faster in the diamond jet than in the round jet. Apparently, this is consistent with the discrepancies in the instantaneous velocity which decays more rapidly in the diamond jet along the x axis. The differences in spreading and decaying (and thus entrainment) between the diamond and round jets are well quantified in the following section by the mean velocity data.

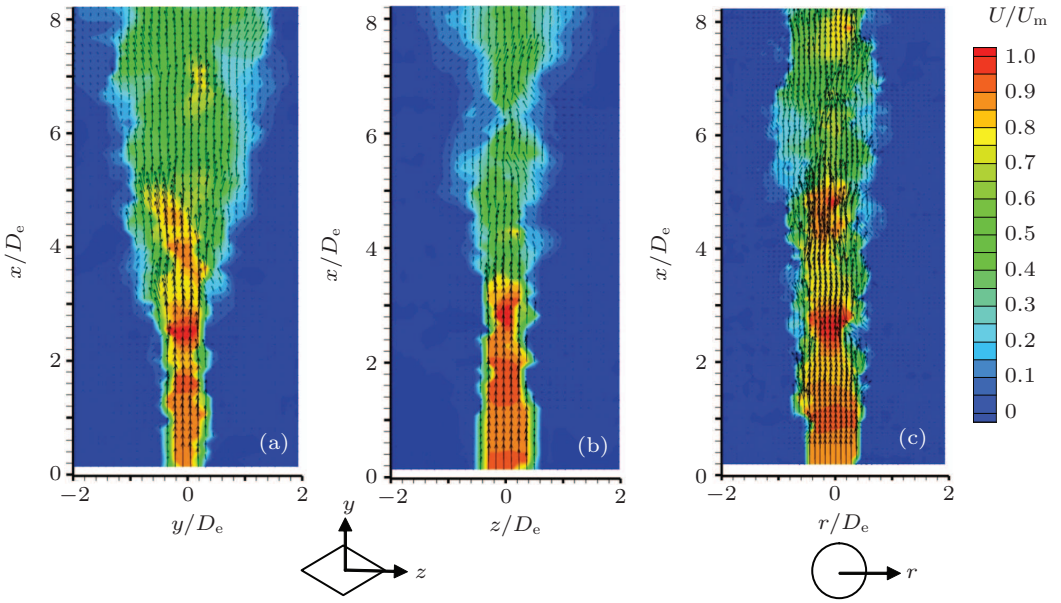

Fig. 2. (color online) Typical instantaneous velocity vectors and contours of their magnitudes in (a) the $x-y$ plane and (b) the $x-z$ plane of the diamond jet, and (c) the central plane of the round jet.

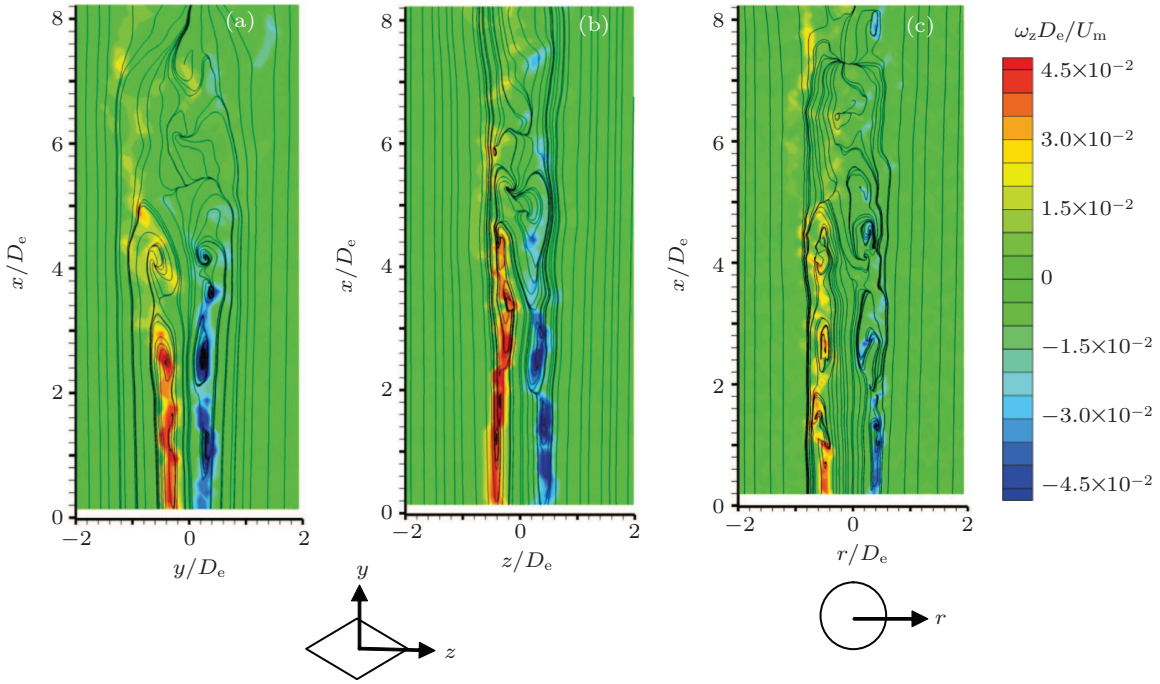

Fig. 3. (color online) Typical instantaneous streamlines in (a) the $x-y$ plane and (b) the $x-z$ plane of the diamond jet, and (c) the central plane of the round jet. The coordinate system translates at a speed of $0.6U_e$ for the two OP jets. Also shown are the spanwise vorticity (ω_z) contours with color-scaled magnitude.

3.2. Mean velocity fields

Figures 4(a) and 4(b) show the normalised mean velocity (U/U_m) contours and mean streamlines in the two symmetric planes of the diamond jet, i.e., the x–y and x–z planes. The comparable view through the central plane of the round jet is presented in Fig. 4(c). These measurement regions span the near-field range approximately of $0 \le x/D_e \le 16$. Also shown (dashed lines) are the locus of the mean-velocity half width, where the mean velocity is half of the centreline velocity, labelled as Ψ_{hw}.

The significant differences between the mean flow fields of the two jets are revealed in Figs. 4(a)–4(c). The diamond jet in the x–z plane contracts slowly from the nozzle exit to $x/D_e \approx 2$, then spreads out continuously further downstream. In contrast, the jet in the x–y plane spreads slowly in the near field of $0 \le x/D_e \le 2$ and then turns to spread out much more rapidly for $x/D_e \ge 2$. These characters are also reflected in the jet's central region, which is delimited by the half-widths (dashed lines, denoted by Ψ_{hw}). By comparison, the round jet spreads out consistently as it proceeds downstream, but at an apparently lower rate than the diamond jet does in the x–y plane. Moreover, as illustrated by the red to yellow contours in Figs. 4(a)–4(c), the mean velocity of the diamond jet is deduced to decrease with x at a higher rate, yielding a shorter

'unmixed core' (in a mean-flow sense). Here we avoid using the term 'potential core'. Strictly, a potential core is a region of the uniform velocity that is only found in a jet from a smooth contraction nozzle. Based on the above observations, the diamond jet is deduced to spread and decay more rapidly than the round jet, which is better quantified below in Figs. 5 and 6. Thus, it is expected for the diamond jet to have a higher rate of entrainment of the ambient fluid.

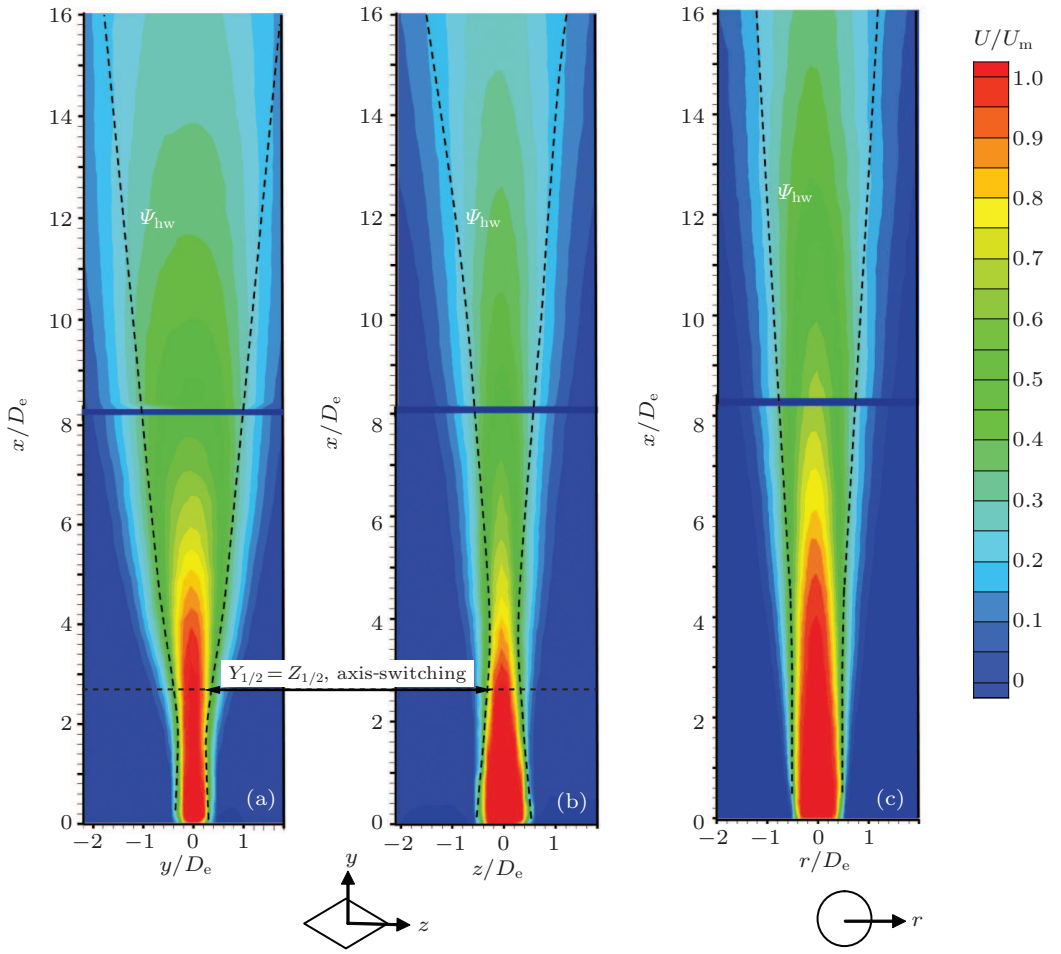

Fig. 4. (color online) Normalized mean velocity (U/U_m) contours in (a) the $x-y$ and (b) $x-z$ planes of the diamond jet, and (c) the central plane of the round jet.

More quantitative evidence in support of the above deductions can be found in Figs. 5 and 6, where the streamwise variations of the normalized centreline velocity (U_c/U_m) and half-velocity widths ($Y_{1/2}$ and $Z_{1/2}$), are shown, respectively. Here, U_m is the maximum of $U_c(x)$ found slightly downstream from the exit plane. It should be noted that normalization by other measures of characteristic velocity, such as the bulk-mean exit velocity, is also feasible. However, U_c/U_m closely approaches unity in the range of $x/D_e \leq 2$ for both nozzles, and so any difference between these two methods of normalization should be negligible. The half width is defined as the lateral location, where the mean velocity is half of the centreline velocity, i.e., $U = 0.5U_c$. For comparison, Figs. 5 and 6 also show the corresponding PIV data for a notched-rectangular jet reported previously by Mi *et al.*[24] and the hot-wire measurements of U_c/U_m for a round orifice jet by Mi and Nathan[23] at $Re \approx 1.5 \times 10^4$ and by Quinn[13] at $Re \approx 2 \times 10^5$. It is worth noting that the magnitudes of U_c and $R_{1/2}$, $Y_{1/2}$, and $Z_{1/2}$ reflect the overall rates of the mean velocity decay and spread.

For the round jet, it is quite evident that the present PIV data are in good agreement with the hot-wire measurements of Mi *et al.*,[23] who used a similar nozzle and experimental apparatus. Thus, this gives confidence in both data sets. However, Quinn's data[13] differ significantly from the present data, especially in the range of $x/D_e < 12$. The discrepancy may be caused by the different upstream flow configurations in the two studies. The present study employed a long pipe to supply the air to the orifice (a configuration more common in industrial applications), while Quinn[13] adopted a smoothly contracting jet facility with a large settling chamber to achieve a uniform, low-turbulence-intensity flow upstream from the orifice. It is interesting to find that the present round jet has a slightly lower decay rate near the end of the potential core than Quinn's, and then the two flows appear to converge to a similar decay rate in the far field. In Fig. 5, it also shows that the mean velocity decay rate of the diamond jet is higher than that of both the round and notched jets, although their final rate cannot be obtained from the present measurements at $x/D_e < 17$. It means that the diamond jet is more effective in entraining the ambient fluid than the notched jet, despite the much larger circumfer-

ence of the notched jet configuration. Also, this suggests that increasing the amount of convolution of the nozzle exit area does not necessarily lead to an increase in entrainment of ambient fluid. Moreover, the length of the unmixed core (L_{pc}) is defined as the x location at which the mean velocity falls below 99% of U_m. For the diamond jet, L_{pc} is shorter than both the notched-rectangular and round jets. The lengths of unmixed core for the diamond, notched-rectangular and round jets are 1.5, 2.2, and 3.5 D_e, respectively.

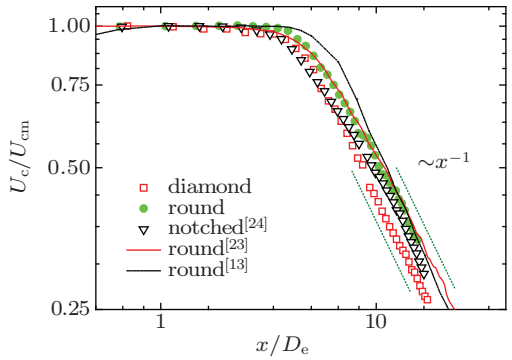

Fig. 5. (color online) Mean velocity decay along the jet centreline (in log-log scale) in the diamond jet in comparison with the round counterpart. Also, the results for the notched jet from Ref. [24] and the round jet from Refs. [13] and [23] are presented.

As shown in Fig. 6, the 'average' spread rate of the diamond jet based on the half-velocity equivalent radius, defined by $R_{eq} = (Y_{1/2}Z_{1/2})^{1/2}$, is greater than the half-velocity radiuses $R_{1/2}$ of the present round jet and the notched-rectangular jet of Mi *et al.*[24] These differences provide further evidence that, overall, the diamond jet has a higher rate of entrainment than the round and also the notched jet cases. Moreover, it is found that the results of the centreline decay are consistent with the spreading rates.

Figure 6 also reveals another interesting feature of the diamond jet, i.e., the 'axis-switching' phenomenon. The half-width of the minor axis (in x–y plane), $Y_{1/2}$, is initially smaller than that of the major axis (in x–z plane), $Z_{1/2}$. Then $Y_{1/2}$ develops to exceed $Z_{1/2}$, i.e., $Y_{1/2} > Z_{1/2}$, at $x > 2.6D_e$. Thus, the switching location is $x \approx 2.6D_e$. The 'axis-switching' location is also shown in Figs. 4(a) and 4(b), where the x-location corresponding to $Y_{1/2} = Z_{1/2}$ (i.e., $x \approx 2.6D_e$) marked by a dashed line and a two-way arrow.

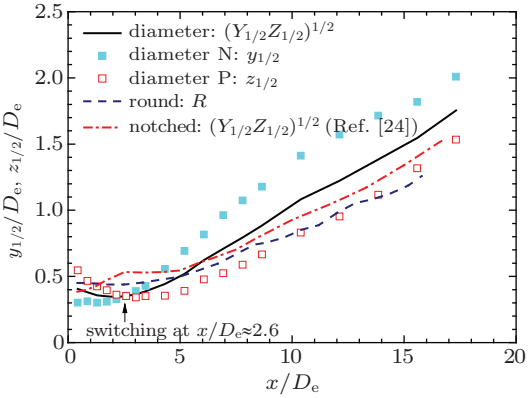

Fig. 6. (color online) Half-velocity widths of the diamond jet in comparison with the round counterpart. Also, the half-velocity width for the notched jet from Ref. [24] is shown

The circular-jet relations for the mean-field self-preservation such as $U_c/U_m \sim x^{-1}$ and $R_{1/2} \sim x$ appear to be approximately valid in the present round and also diamond jet when $x/D_e \approx 8$, as Figs. 5 and 6 present. However, satisfying these relations does not necessarily imply that the mean flow has achieved a self-preserving state, and also that the initially 'diamond' shape of the jet has statistically become a 'round' one. To achieve the self-preservation, it requires the collapse of the lateral normalized profiles of the mean velocity (U) by the centreline or maximum value (U_c) at any value of x, i.e., $U/U_c = f(\eta)$, where $\eta = r/R_{1/2}$, $y/Y_{1/2}$ or $z/Z_{1/2}$. Figures 7(a)–7(c) present these profiles for both the diamond and round jets. The far-field distribution of U/U_c obtained by Hussein *et al.*[31] in a round jet issuing from a smooth contraction nozzle and the Gaussian distribution $U/U_c = \exp(-\eta^2 \ln 2)$ are also shown in Figs. 7(a)–7(c). It is interesting to note that, for $x/D_e \approx 8$, the radial profiles of U/U_c for the round jet collapse well with the Gaussian and Hussein *et al.*'s distributions (both differing slightly). Considering Figs. 5–7 together, we conclude that the mean flow of the round jet has achieved a self-preserving state approximately at $x/D_e \approx 8$. However, this conclusion cannot apply to the diamond jet whose axes switch at $x \approx 2.6D_e$. While the profiles in the x–z plane exhibit a good agreement with Hussein *et al.*'s distribution, the profiles in the x–y plane do not. The self-preservation of the diamond jet requires the mean flow to be axisymmetric, which can only occur much further downstream from the location of the last axis-switching.

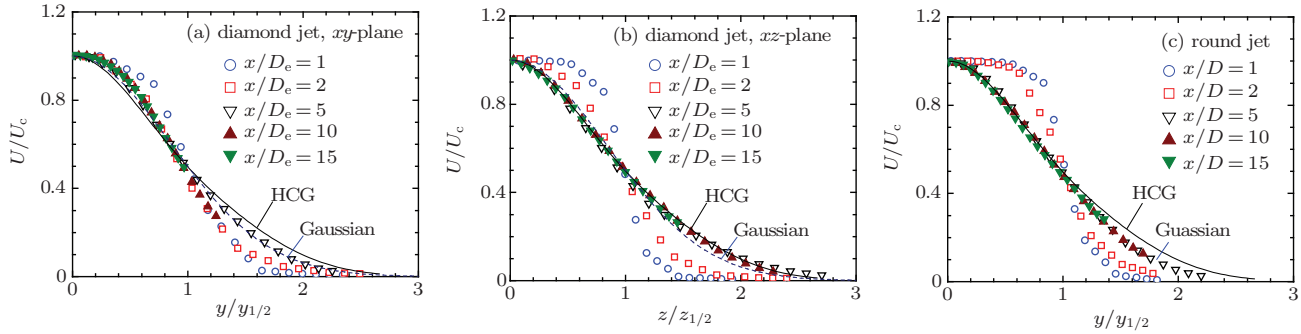

Fig. 7. (color online) Lateral profiles of the normalized mean velocity (U/U_c) in (a) the $x-y$ plane and (b) the $x-z$ plane of the diamond jet, and (c) the central plane of the round jet. The HCG denotes Hussein, Capp, and George.[31]

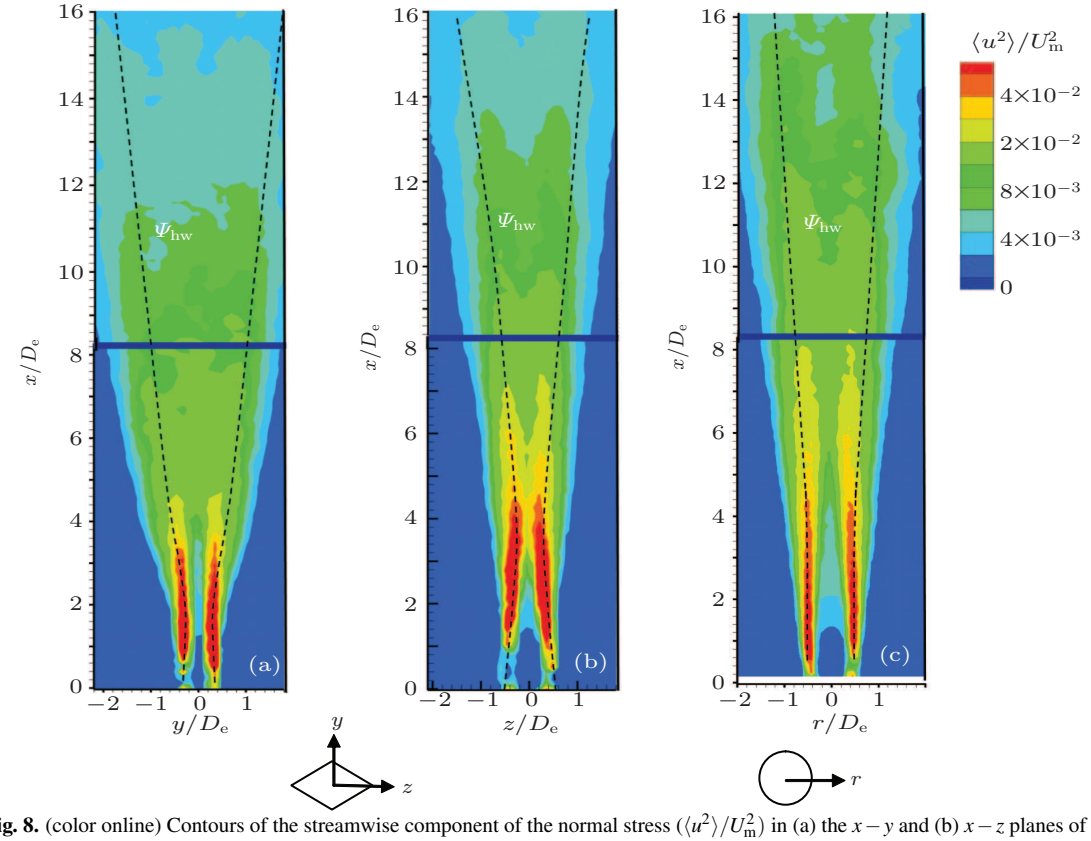

Fig. 8. (color online) Contours of the streamwise component of the normal stress ($\langle u^2\rangle/U_m^2$) in (a) the $x-y$ and (b) $x-z$ planes of the diamond jet, and (c) in the central plane of the round jet.

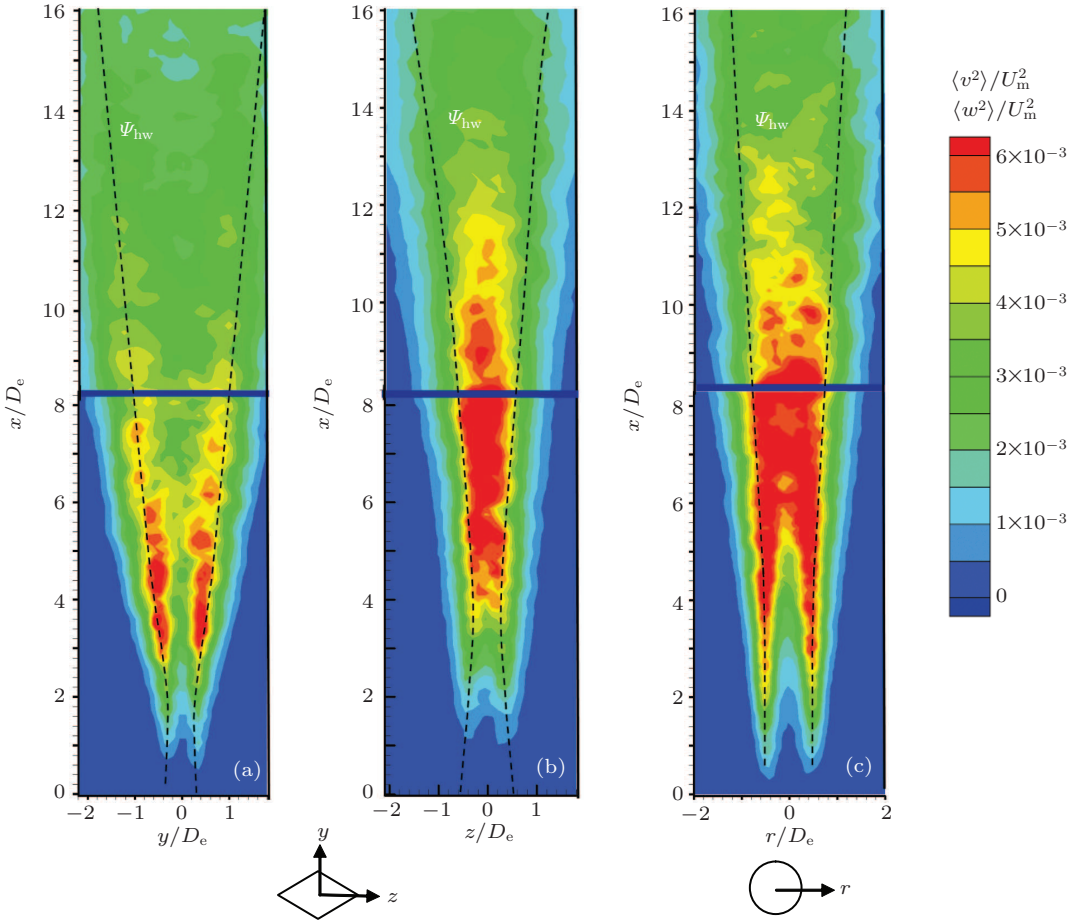

Fig. 9. (color online) Contours of the lateral components of the normal stress. (a)$\langle v^2\rangle/U_m^2$ in the x–y plane of the diamond jet, (b) $\langle w^2\rangle/U_m^2$ in the $x-z$ plane of the diamond jet, and (c) $\langle v^2\rangle/U_m^2$ in the central plane of the round jet.

3.3. Reynolds normal and shear stresses

Figures 8–10 show contours of the Reynolds normal and shear stresses normalized by the maximum velocity U_m, i.e., $\langle u^2\rangle/U_m^2$, $\langle v^2\rangle/U_m^2$, and $\langle uv\rangle/U_m^2$ in the x–y plane; $\langle u^2\rangle/U_m^2$, $\langle w^2\rangle/U_m^2$, and $\langle uw\rangle/U_m^2$ in the x–z plane of the diamond jet and in the central plane of the round jet, for $x/D_e \leq 16$. The half-width locus, Ψ_{hw}, is also shown as a reference. Several observations can be made from these plots.

Firstly, the highest values of $\langle u^2\rangle/U_m^2$ are consistently located near the half-widths in both the $x-y$ and $x-z$ planes for the diamond jet (Figs. 8(a) and 8(b)) and near the half-radius of the central plane for the round jet (Fig. 8(c)). The corresponding locations for the maxima of $\langle v^2\rangle/U_m^2$ in the x–y plane for the diamond jet appear to shift slightly inward (Fig. 9(a)), while those locations for the maxima of $\langle w^2\rangle/U_m^2$ in the x–z plane for the diamond jet move towards the centreline (Fig. 9(b)). In contrast, as the jet flow developing downstream from the exit plane, those locations for the maxima of $\langle v^2\rangle/U_m^2$ or $\langle w^2\rangle/U_m^2$ in the central plane for the round jet gradually shift to the axis (Fig. 9(c)). Apparently, the off-axis peak of $\langle u^2\rangle/U_m^2$ is more distinct than those of $\langle v^2\rangle/U_m^2$ and $\langle w^2\rangle/U_m^2$ across the jet.

Secondly, the absolute value of the shear stress in both jets reaches its maximum around Ψ_{hw} in the very near field, and the maximum shifts inward further downstream in both measurement planes. The above behaviors of the Reynolds normal and shear stresses are associated with the mean shears ($\partial U/\partial y$ and $\partial U/\partial z$) whose maxima are located also around the half-widths in the near field but move to an inner location at $y \approx 0.8Y_{1/2}$ or $z \approx 0.8Z_{1/2}$ at $x/D_e > 10$ (not shown here). Hence, both the jet half-widths and maximal Reynolds stresses take place around the maximal mean shears, regardless the generation of the turbulent jets. Perhaps it is also worth noting that the relatively poor PIV resolution in near field of the jet caused less satisfactory results of Reynolds stresses, especially $\langle v^2\rangle$ and $\langle w^2\rangle$ for $x/D_e < 3$.

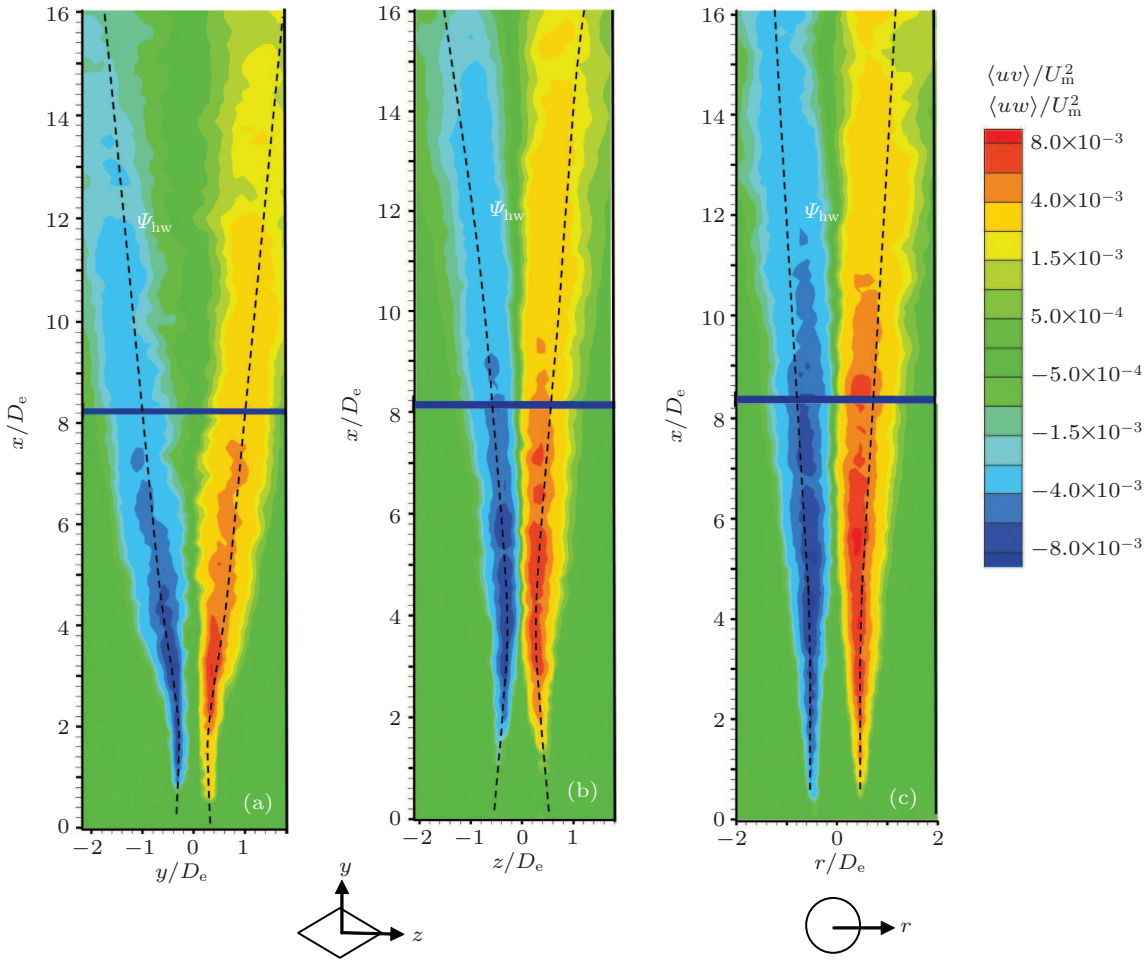

Fig. 10. (color online) Contours of the normalized Reynolds shear stress. (a) $\langle uv\rangle/U_m^2$ in the x–y plane of the diamond jet, (b) $\langle uw\rangle/U_m^2$ in the x–z plane of the diamond jet, and (c) $\langle uv\rangle/U_m^2$ in the central plane of the round jet.

4. Conclusions

The first investigation into the velocity field of a diamond turbulent jet has been undertaken using planar PIV measurements, from which we draw the following conclusions.

1) The primary coherent structures in the diamond jets break down more rapidly than in the round jet, due to a higher three-dimensionality of the near-field underlying flow.

2) The diamond jet exhibits a significantly higher rate of

entrainment of the ambient fluid than the comparable round jet does. This is reflected by the shorter unmixed core, higher rates of decay, and spread of the mean velocity for the diamond jet relative to the round jet.

3) The phenomenon of axis switching occurs in the present diamond jet (at $x \approx 2.6D_e$ for the present aspect ratio of 1.7), and the asymmetry persists throughout the measured range. Another axis-switching event is expected to occur further downstream, beyond the present measurement region, namely, $x/D_e > 17$.

4) Although the self-preserving relations $U_c/U_m \sim x^{-1}$ and $R_{1/2} \sim x$ appear to be met at $x/D_e \geq 8$ in the round jet, the mean flow of the diamond jet is far from exhibiting self-preservation even at $x/D_e = 17$.

5) Generally, in both jets under investigation, the Reynolds stresses $\langle u^2 \rangle$, $\langle uv \rangle$, and $\langle uw \rangle$ reach their maxima around the location of the maximal mean shear, while the maxima of $\langle v^2 \rangle$ and $\langle w^2 \rangle$ appear around the centreline in any measurement plane. The maxima of the mean shears ($\partial U/\partial y$ and $\partial U/\partial z$) occur around the half widths in the very near field, which however shift to $y \approx 0.8Y_{1/2}$ or $z \approx 0.8Z_{1/2}$ further downstream for $x/D_e > 10$.

Acknowledgements

It is acknowledged that the PIV measurements were performed at the University of Adelaide with the support of the Australian Research Council.

References

[1] Gutmark E, Schadow K, Parr T, Hanson-Parr D and Wilson K 1989 *Expt. Fluids* **7** 248
[2] Schadow K, Gutmark E, Parr D and Wilson K 2004 *Expt. Fluids* **6** 129
[3] Ho C and Gutmark E 1987 *J. Fluid Mech.* **179** 383
[4] Hussain F and Husain H 1989 *J. Fluid Mech.* **208** 257
[5] Husain H and Hussain A 1983 *Phys. Fluids* **26** 2763
[6] Koshigoe S, Gutmark E, Schadow K and Tubis A 1989 *AIAA J.* **27** 411
[7] Gollahalli S R, Khanna T and Prabhu N 1992 *Combust. Sci. Technol.* **86** 267
[8] Tam C K W and Thies A T 1993 *J. Fluid Mech.* **248** 425
[9] Grinstein F, Gutmark E and Parr T 1995 *Phys. Fluids* **7** 1483
[10] Miller R, Madnia C and Givi P 1995 *Comput. Fluids* **24** 1
[11] Quinn W R 2007 *Eur. J. Mech. B* **26** 583
[12] Quinn W R 2005 *Eur. J. Mech. B* **25** 279
[13] Quinn W R 1994 *AIAA J.* **32** 547
[14] Quinn J 1989 *Int. J. Heat Fluid Flow* **10** 139
[15] Zaman K 1999 *J. Fluid Mech.* **383** 197
[16] Zaman K B M Q 1996 *J. Fluid Mech.* **316** 1
[17] Deo R C, Mi J and Nathan G J 2007 *Exp. Therm. Fluid Sci.* **32** 545
[18] Deo R C, Mi J and Nathan G J 2007 *Exp. Therm. Fluid Sci.* **31** 825
[19] Mi J and Nathan G J 1999 *Int. J. Heat Mass Transfer* **42** 3919
[20] Mi J, Nathan G J and Luxton R E 2000 *Expt. Fluids* **28** 93
[21] Mi J, Deo R C and Nathan G J 2005 *Phys. Fluids* **17** 068102
[22] Mi J, Kalt P, Nathan G J and Wong C Y 2007 *Expt. Fluids* **42** 625
[23] Mi J and Nathan G 2010 *Flow Turbulence Combust.* **84** 583
[24] Mi J, Kalt P and Nathan G 2010 *Flow Turbulence Combust.* **84** 565
[25] Du C, Xu M and Mi J 2010 *Acta Phys. Sin.* **59** 6323 (in Chinese)
[26] Mi J and Du C 2011 *Chin. Phys. B* **20** 124701
[27] Xu M, Du C and Mi J 2011 *Acta Phys. Sin.* **60** 34701 (in Chinese)
[28] Mi J C and Feng B P 2011 *Chin. Phys. B* **20** 074701
[29] Gutmark E and Grinstein F 1999 *Annu. Rev. Fluid Mech.* **31** 239
[30] Hussain A and Clark A 1981 *J. Fluid Mech.* **104** 263
[31] Hussein H, Capp S and George W 1994 *J. Fluid Mech.* **258** 31